

Supplementary information

Quality of Graphene on Sapphire: Long-range Order from Helium
Diffraction versus Lattice Defects from Raman Spectroscopy

Gloria Anemone,¹ Esteban Climent-Pascual,² Hak Ki Yu,^{3,4}
Amjad Al Taleb,¹ Felix Jiménez-Villacorta,² Carlos Prieto,²
Alec M. Wodtke,^{3,4} Alicia De Andrés,² and Daniel Farías^{1,5,6}

¹*Departamento de Física de la Materia Condensada,
Universidad Autónoma de Madrid, 28049 Madrid, Spain*

²*Instituto de Ciencia de Materiales de Madrid.*

Consejo Superior de Investigaciones Científicas, Spain

³*Institute for Physical Chemistry, University of Göttingen, 37077 Göttingen, Germany*

⁴*Max Planck Institute for Biophysical Chemistry, 37077 Göttingen, Germany*

⁵*Instituto "Nicolás Cabrera", Universidad Autónoma de Madrid, 28049 Madrid, Spain*

⁶*Condensed Matter Physics Center (IFIMAC),
Universidad Autónoma de Madrid, 28049 Madrid, Spain*

(Dated: February 10, 2016)

EXPERIMENTAL DETAILS

Experimental setup

The samples were characterized *in situ* by Helium Atom Scattering (HAS) and *ex situ* by atomic force microscopy (AFM), Raman spectroscopy and optical transmission. The HAS experiments have been carried out in a high-resolution He-scattering machine with a fixed 105.7° source-target-detector geometry [1, 2]. The He diffraction measurements were performed with a source pressure of 80 bar behind a $10\ \mu\text{m}$ platinum nozzle. The beam energy used in the current work was 19.8 meV, with a corresponding energy spread of 2.5%. Atomic force microscopy (AFM) characterization was carried out in the tapping mode using a microscope head and software from Nanotec [3]. Commercial PPP-NCH-w tips, with resonance frequency of about 270 kHz and spring constant around $34\ \text{Nm}^{-1}$ (between 10 and $100\ \text{Nm}^{-1}$), adequate for dynamic mode, were utilized to collect topographic images, as well as amplitude and phase mappings. Several areas in different regions were checked (for every sample). Micro-Raman experiments were performed at room temperature using the 488 nm line of an Ar^+ laser (incident power around 8 mW) with an Olympus microscope ($\times 100$ objective) of very high numerical aperture, $\text{NA}=0.95$ and a "super-notch-plus" filter from Kaiser. The scattered light was analyzed with a Jobin-Yvon HR-460 monochromator coupled to a Peltier cooled Synapse CCD. Raman spatial resolution is estimated to be around $0.8\ \mu\text{m}$. Raman images of different sizes ($20 \times 10\ \mu\text{m}^2$ and $10 \times 10\ \mu\text{m}^2$) and $1\ \mu\text{m}$ steps as well as individual spectra were obtained. Optical images of the same areas were also collected.

AFM

Fig. SI3 shows AFM topographic images in two representative areas on the sample with initially thickness of 500 nm Cu film. Images reveal the presence of dispersed graphene flakes of size $0.2\text{-}0.4\ \mu\text{m}$ on at sapphire substrate between the Cu micrometric islands. Fig. SI4 shows an estimation of the coverage of graphene on the sapphire substrate. In Fig. SI5 the estimation of the rms roughness in graphene layers and the substrate is illustrated. Finally, Fig. SI6 shows the location of nanometric pits in the sapphire substrate observed in the dynamic (tapping) and contact (provoking removal of the graphene layer) modes.

Raman spectra

In Figure SI-7 the Raman spectra of as deposited graphene on Cu/Al₂O₃ and of graphene after the elimination of the 1000 nm copper film are presented. In order to correlate ID/IG and the distance between the defects, L_D the following equation has been used [4]:

$$\frac{I_D}{I_G} = C_A \frac{(r_A^2 - r_S^2)}{(r_A^2 - 2r_S^2)} [e^{-\pi r_S^2/L_D^2} - e^{-\pi(r_A^2 - r_S^2)/L_D^2}] \quad (1)$$

The optical image of a $10 \times 10 \mu\text{m}^2$ area of Sample 1, is replicated by the Raman image of the background due to Cu (2000-2500 cm^{-1} region) (Fig. SI8 upper panels) allowing to identify when graphene is on Cu and when it is on sapphire (Fig. SI8-c). This area is representative of the several measured Raman images. The intensity of G peak is higher in for graphene on copper residues than on sapphire (Fig. SI8-e) indicating that in these regions graphene is partially eliminated. Nevertheless, the ID/IG and I2D/IG (Fig. SI8 d and f) are quite uniform across the images indicating a similar quality of the graphene layer independently of the presence of Cu. The clear frequency increase of 2D peak for graphene on sapphire compared to that on copper (Fig. SI8 g) indicates different interaction with the substrate leading to changes in graphene doping.

-
- [1] Ernst, H. J.; Hulpke, E. and Toennies, J. P. Helium-atom-scattering study of the structure and phonon dynamics of the w(001) surface between 200 and 1900 K. *Phys. Rev. B*, 1992, **46**, 16081-16105.
- [2] Barredo, D.; Laurent, G.; Nieto, P.; Farías, D. and Miranda. R. High-resolution elastic and rotationally inelastic diffraction of D₂ from NiAl(110). *J. Chem. Phys.*, 2010, **133**, 124702.
- [3] I. Horcas, R. Fernandez, J.M. Gómez-Rodríguez, J. Colchero, J. Gómez-Herrero and A.M. Baró, *Rev. Sci. Instrum.* , 2007, **78**, 013705.
- [4] Lucchese, M. M.; Stavale, F.; Ferreira, E. H. M.; Vilani, C.; Moutinho, M. V. O.; Capaz, R. B.; Achete, C. a.; Jorio, a. Quantifying Ion-Induced Defects and Raman Relaxation Length in Graphene. *Carbon*, 2010, **48**, 1592–1597.

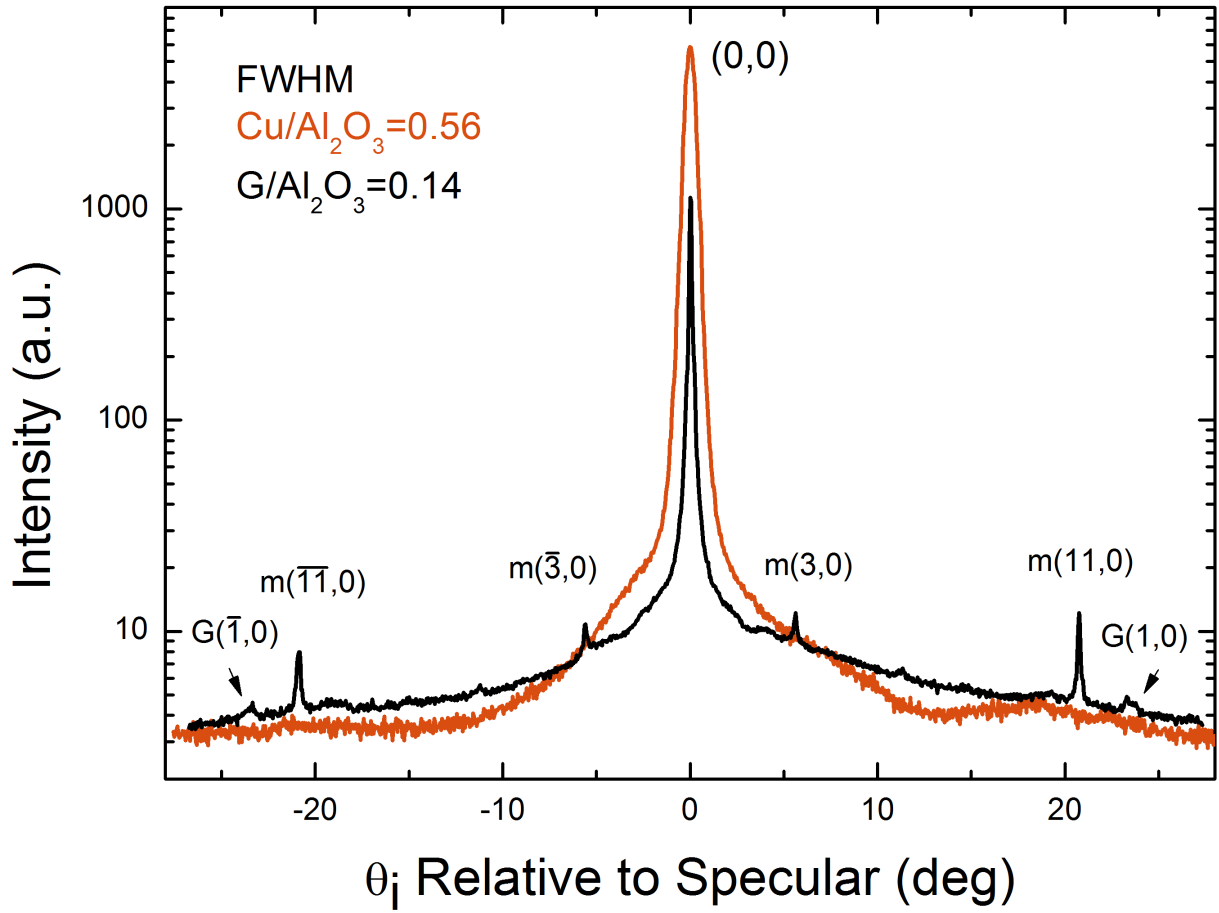


FIG. 1: Comparison of He diffraction spectra from Gr/Al₂O₃ (black) and Cu/Al₂O₃ (red). The sample temperature is 90 K, and the He-incident energy is $E_i = 19.8$ meV.

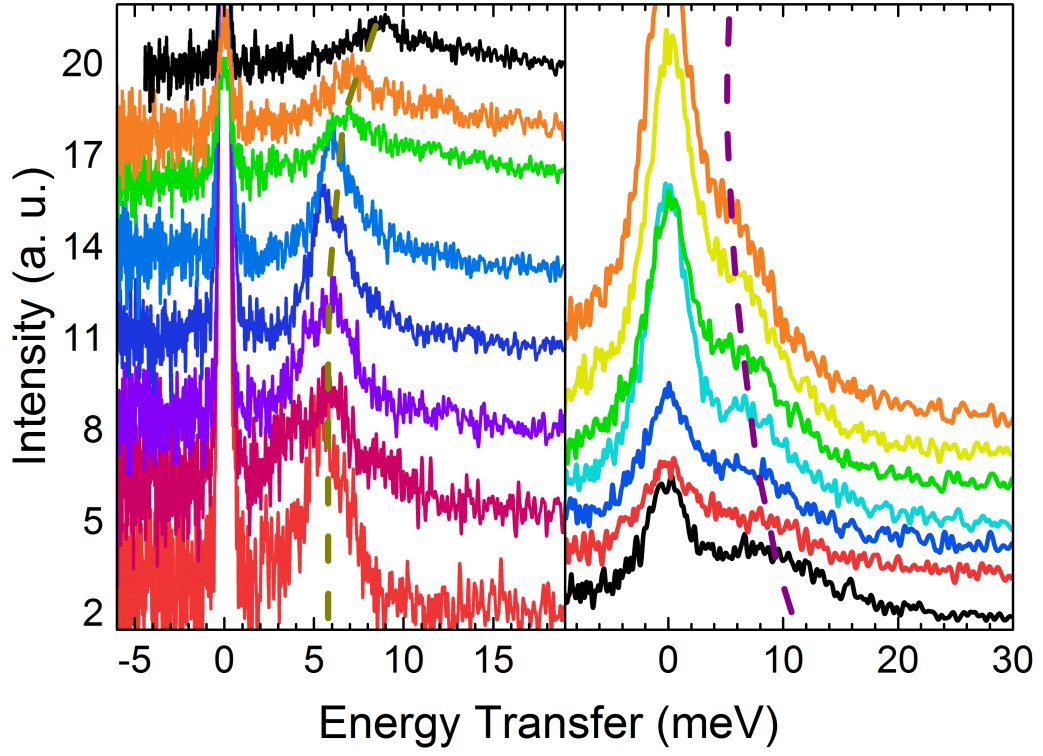


FIG. 2: Time-of-flight spectra of He scattered from Gr/ Al_2O_3 for two different incident energies $E_i = 21.5$ meV (left) and $E_i = 67.5$ meV (right).

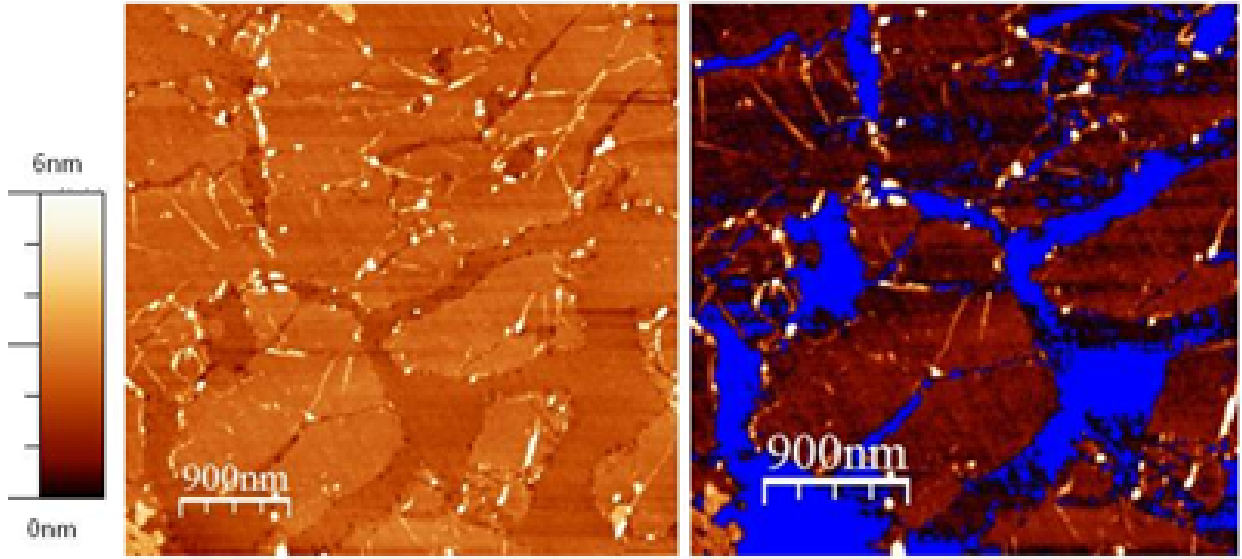


FIG. 3: Illustrative example of the estimation of the sapphire coverage by the graphene layers (in this case $\sim 80\%$), using the flooding analysis (flood height: 1.8 nm).

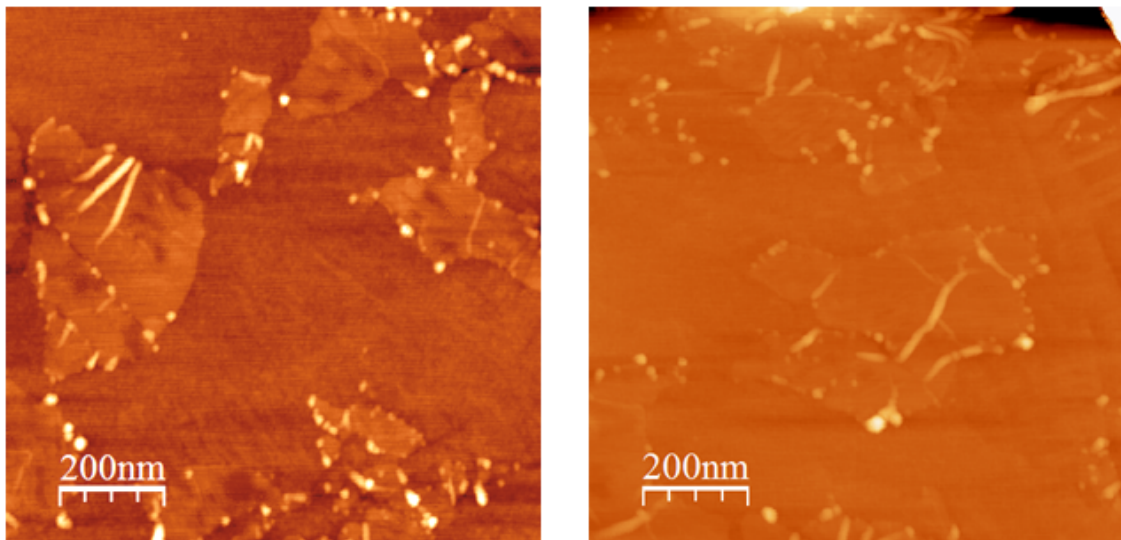


FIG. 4: AFM topographic images of graphene/sapphire (Sample with initially 500 nm Cu film). Image $1 \mu\text{m} \times 1 \mu\text{m}$.

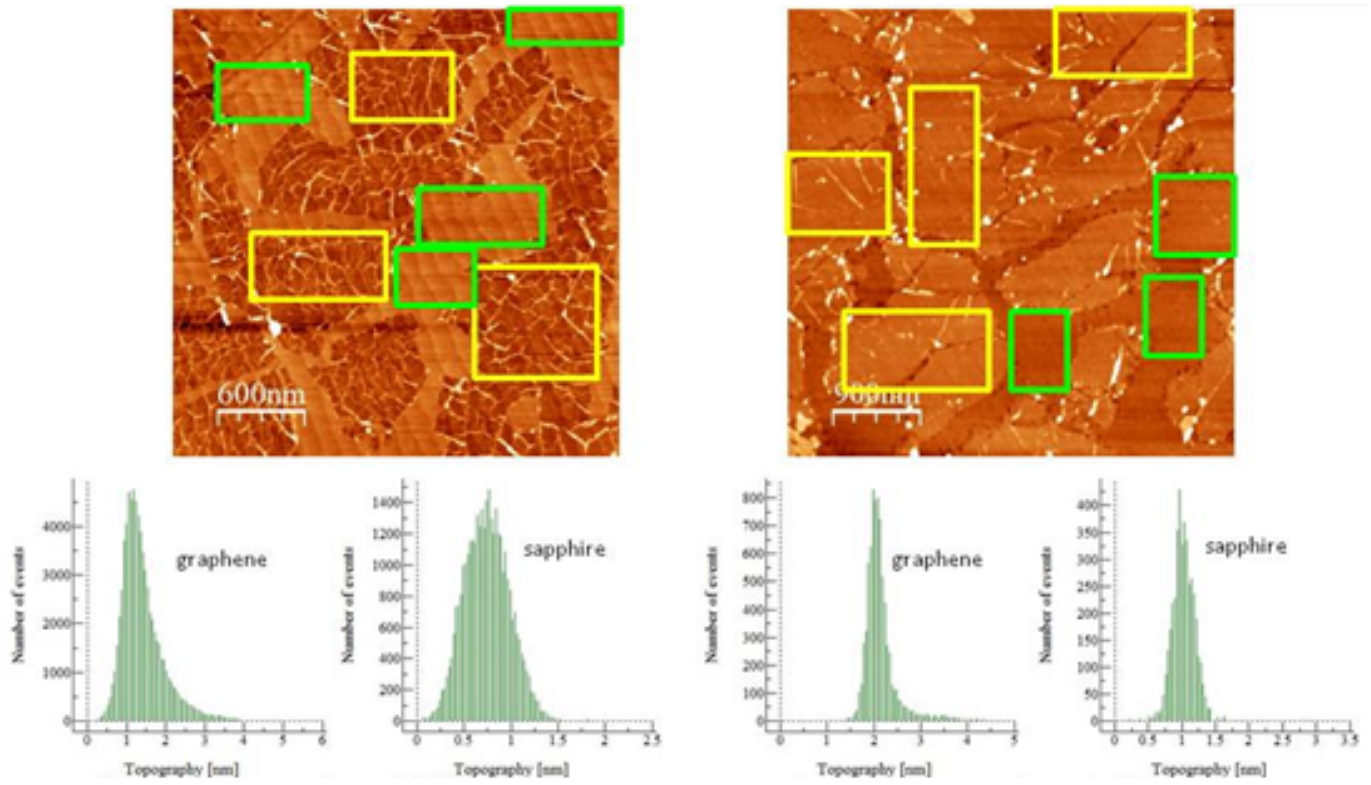


FIG. 5: Example describing the estimation of the *rms* roughness (using height histograms) in the graphene layers and the substrate. Several graphene-covered areas (yellow rectangles) and bare substrate areas (green rectangles) were selected for the roughness analysis.

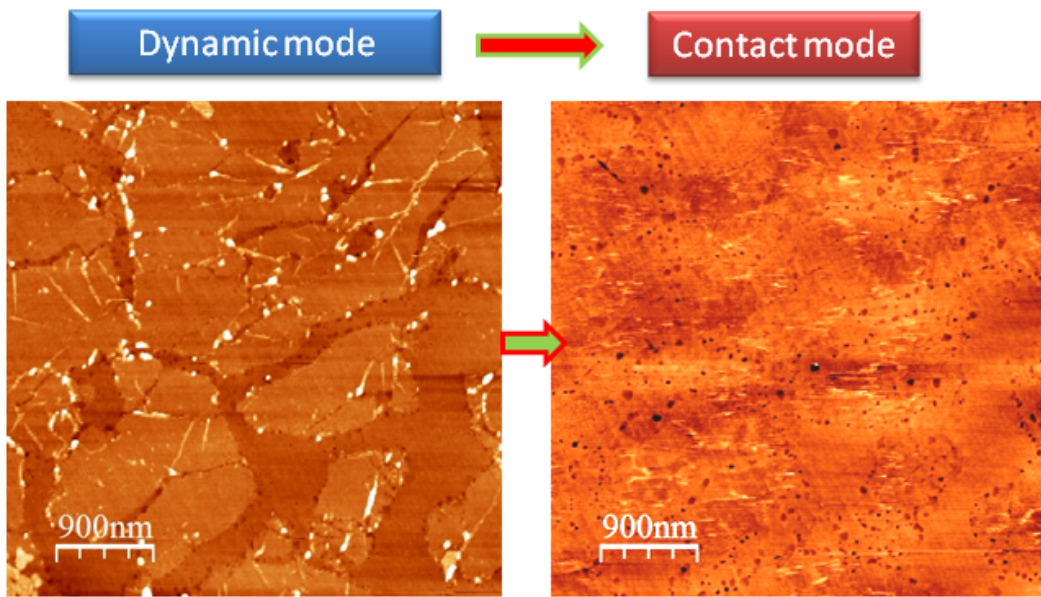


FIG. 6: Comparison between the topographic images in the dynamic tapping mode and in the contact mode (the normal force mapping of the same area was also represented), revealing that the pit distribution is mainly confined at the graphene domain boundaries.

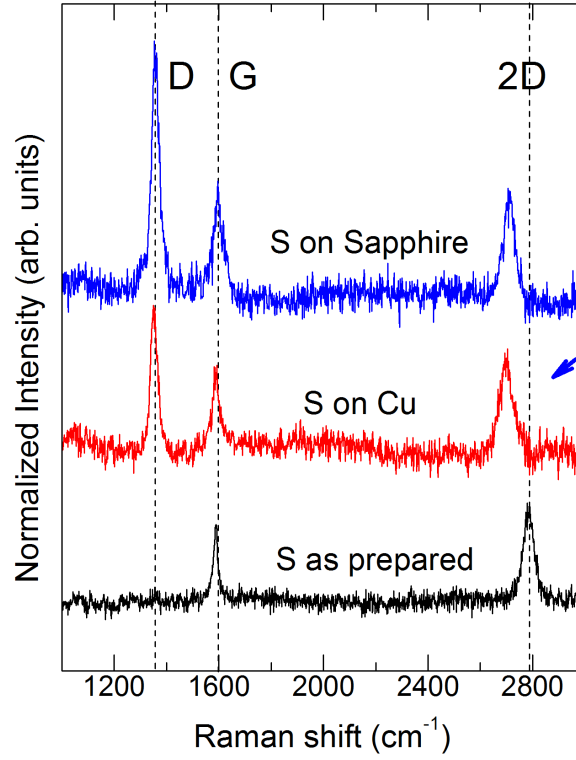


FIG. 7: Raman spectra of the sample with 1000 nm Cu film as deposited (S as prepared) and after annealing either on remaining Cu microstructures (S on Cu) or on sapphire (S on Sapphire). The background due to copper has been eliminated for clarity. D, G and 2D characteristic peaks of graphene are indicated.

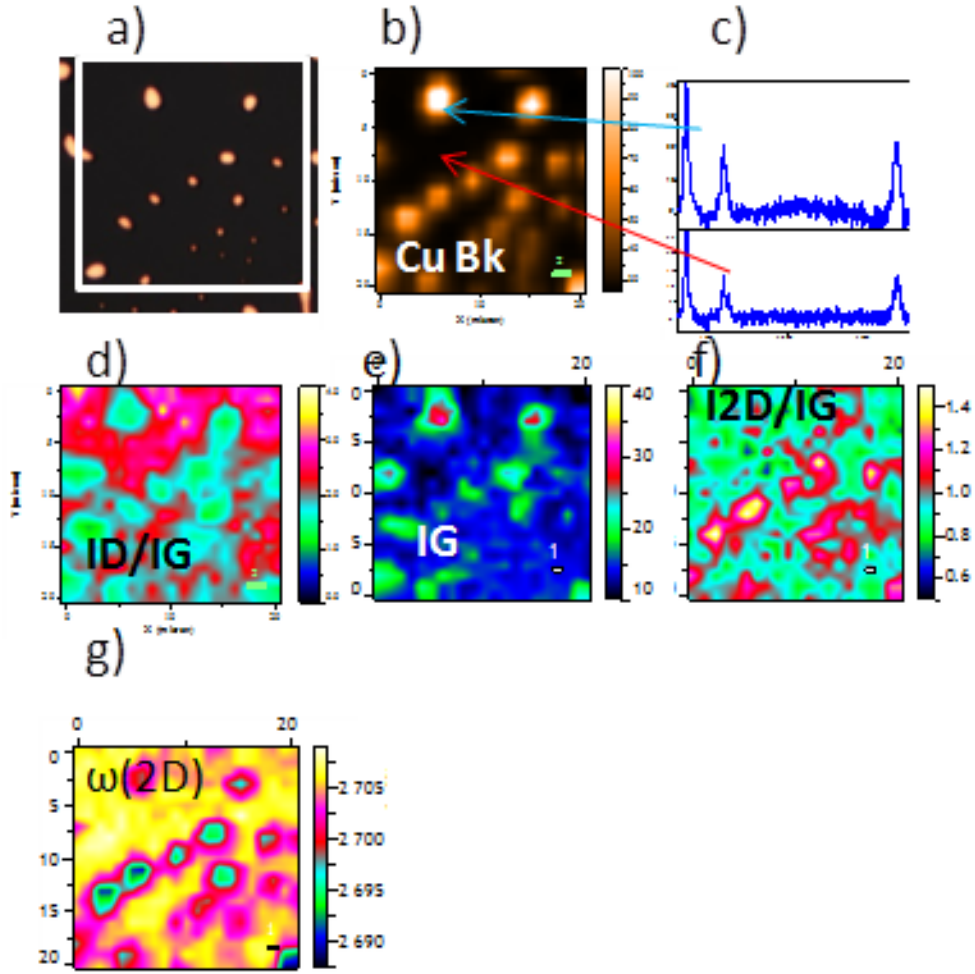


FIG. 8: Sample with 500 nm Cu film: a) Optical image, b) Raman image ($10 \times 10 \mu m^2$) of the background revealing the Cu residues c) spectra at two positions (Cu background substrated) d) ID/IG, e) IG and f) I2D/IG Raman images. g) Raman image of the frequency of 2D peak.